Transcription-replication coordination revealed in single live cells

Ioannis Tsirkas[1,†], Daniel Dovrat[1,†], Manikandan Thangaraj[2], Ineke Brouwer[3], Amit Cohen[1], Zohar Paleiov[1], Michael M. Meijler[2], Tineke Lenstra[3] and Amir Aharoni [1,*,‡]

[1]Department of Life Sciences, Ben-Gurion University of the Negev, Be'er Sheva 84105, Israel, [2]The Department of Chemistry and the National Institute for Biotechnology in the Negev, Ben-Gurion University of the Negev, Be'er Sheva 84105, Israel and [3]Division of Gene Regulation, The Netherlands Cancer Institute, Oncode Institute,1066CX Amsterdam, The Netherlands

ABSTRACT

The coexistence of DNA replication and transcription during S-phase requires their tight coordination to prevent harmful conflicts. While extensive research revealed important mechanisms for minimizing these conflicts and their consequences, little is known regarding how the replication and transcription machinery are coordinated in real-time. Here, we developed a live-cell imaging approach for the real-time monitoring of replisome progression and transcription dynamics during a transcription-replication encounter. We found a wave of partial transcriptional repression ahead of the moving replication fork, which may contribute to efficient fork progression through the transcribed gene. Real-time detection of conflicts revealed their negative impact on both processes, leading to fork stalling or slowdown as well as lower transcription levels during gene replication, with different trade-offs observed in defined subpopulations of cells. Our real-time measurements of transcription-replication encounters demonstrate how these processes can proceed simultaneously while maintaining genomic stability, and how conflicts can arise when coordination is impaired.

INTRODUCTION

DNA contains the genetic information of the cell that must be preserved and replicated during cell growth and division. During DNA replication, cells need to maintain and promote additional cellular processes, including cell cycle progression and energy production, through the expression of hundreds of genes (1,2). Consequently, cells carefully coordinate replication fork progression and transcription dynamics during genome duplication to prevent conflicts between the replication and transcription machinery. Nevertheless, harmful conflicts can take place during S-phase leading to replisome stalling, DNA damage and genomic instability (3–6). These transcription-replication conflicts (TRCs) can occur when the replisome moves in the same or in the opposite direction of RNA polymerases (RNAPs), referred to as codirectional (CoD) or head-on (HO) collision orientations, respectively, where the latter is considered as more detrimental (7–9).

In the past decades, extensive research revealed a variety of mechanisms for minimizing TRCs in different organisms including bacteria, yeast and mammalian cells (3–5). These mechanisms can act directly to prevent collision of the moving replisome with RNAP or indirectly by overcoming different transcription-associated obstacles hindering replisome progression. Specific mechanisms that reduce TRC levels in cells include RNAP eviction during DNA replication, relaxation of topological stress accumulated between the moving replisome and RNAPs and elimination of R-loops formed by the hybridization of the transcribed RNAs with the DNA template. Accordingly, mutations in key proteins including RNAPII (10), topoisomerases (Top1/2) (11,12), Sen1 DNA:RNA helicase (13–15) and RNaseH (16–18) lead to increased levels of harmful TRCs and genomic instability. Some of these mutations were shown to be associated with different pathological conditions including cancer development and neurodegenerative diseases (3,6).

While many studies investigated the consequences of TRCs on genomic stability (3–5), little is known regarding the mechanism of coordination between replisome progression and transcriptional activity to prevent and resolve TRCs and how mutations that increase TRC levels alter such coordination. Specifically, it is unknown how replisome progression influences gene transcription prior, during and following replication of the transcribed gene. Whereas TRC events that lead to genomic instability are

---

usually rare (8,10), it is not clear whether transcription-replication encounters commonly affect replisome progression and transcription dynamics, particularly when forks traverse highly transcribed regions. Finally, little is known regarding potential trade-offs between replisome progression rates and transcription levels during TRCs, and how they might relate to heterogeneity in cellular behavior.

Here, we have developed and utilized a live-cell microscopy approach for the real-time monitoring of both replication and transcription at the same locus during a transcription-replication encounter in single *Saccharomyces cerevisiae* cells. The approach enables high-resolution measurements of replisome progression rates and transcription levels while the replisome progresses through the inducible *GAL10* gene. Using this approach, we found that *GAL10* transcription is partially repressed ahead of the moving replisome, and replisome progression through the gene is not hindered by transcription. However, in the presence of excessive RNAPII accumulation on chromatin, we detected abundant conflicts leading to fork stalling or slowdown and transcriptional repression. Examination of topoisomerase I deficient cells showed a trade-off between replication and transcription, highlighting the detrimental effect of topological stress on the coordination between these processes. Overall, these results reveal tight coordination between replication and transcription that is dependent on proper eviction of RNA polymerase from actively transcribed genes and prevention of topological stress.

MATERIALS AND METHODS

Strain generation

Strains for replisome tracking and *GAL10* transcription monitoring were generated on the background of W1588, which is identical to W303 but with a wild-type copy of Rad5, MATa *S. cerevisiae* strain, expressing LacI-HaloTag, tetR-tdTomato and PCP-Envy fusion proteins in the nucleus. *LacO*x256 and *TetO*x224 arrays are located at *chrIV*:332960 and *chrIV*:352560 respectively, adjacent to *ARS*413. The *GAL10* gene cassette, labeled with 14xPP7 repeats between its 404 bp promoter and its ORF and flanked by *CUT60* terminator sequences, was inserted between the two arrays, either at *chrIV*:336186 (origin-proximal with a mid-array distance of 34 kb) or in *chrIV*:352533 (origin-distal with a mid-array distance of 35.7 kb), in either CoD or HO orientation relative to the progression of a replisome emanating from *ARS413*. In the case of *PP7-GAL10* construct insertion at the *URA3* locus, the location of integration was *chrV*:116167. All *PP7-GAL10* integrations were performed using a markerless CRISPR-Cas9 approach, by targeting *natMX* or *hphMX* antibiotic cassettes with specific gRNAs (19). Strain for the examination of DSB between the *lacO* and *tetO* arrays was generated by the introduction of a fragment from *hphMX* antibiotic cassette between the arrays followed by the integration of live Cas9 and gRNA targeting the *hphMX* sequence into the *URA3* locus using an integrative plasmid. The *rpb1-1* mutant strains harboring the G4622A mutation (10) were generated with CRISPR-Cas9, using a gRNA which targets the *RPB1* gene close to the mutated region (gRNA sequence: AGTTGGA-GAAAAGCCTGGTG) and DNA donor containing the

mutation, with 75 bp homology to the genome on each side of the targeted region. Mutant *rpb1-1* strain was validated by polymerase chain reaction (PCR), Sanger sequencing and sensitivity to methyl methanesulfonate (MMS). To generate the *top1Δ* strains, the *TOP1* gene was replaced by *natMX* antibiotic cassette. *SMC1*-AID strains were generated by integrating a PCR cassette containing the degron sequence followed by 6xFLAG-Tag, *hphMX* antibiotic cassette and the *Oryza sativa* TIR1 gene at the 3' end of the *SMC1* gene (20). All replacements and integrations were validated by PCR.

SiR-Halo dye synthesis

The synthesis of 2-(2-((6-chlorohexyl)oxy)ethoxy)ethana mine (compound 1) reactive group for the covalent labeling of the Halo protein tag was performed in three steps, as previously described (21). Briefly, the amine group of 2-(2-aminoethoxy)ethanol was protected by a Boc protecting group to generate the *tert*-butyl (2-(2-hydroxyethoxy)ethyl)carbamate. Next, the hydroxy group of the *tert*-butyl (2-(2-hydroxyethoxy)ethyl)carba mate was reacted with 6-chloro-1-iodohexane to generate the *tert*-butyl (2-(2-((6-chlorohexyl)oxy)ethoxy)ethyl) carbamate. Finally, Boc deprotection to generate compound 1 was performed in a mixture of dichloromethane (DCM)/trifluoroacetic acid (TFA) followed by purification. The synthesis of the SiR-Halo-dye was performed by reacting the SiR-carboxyl (Spirochrome) with compound 1 under basic conditions followed by reverse phase HPLC purification, as previously described (22). All synthesis steps were verified by NMR and mass spectroscopy analysis for SiR-Halo-dye. Stock solutions of SiR-Halo-dye were prepared by diluting the dye to a final concentration of 400 μM in DMSO.

Microscopy

Yeast cells were grown overnight in synthetic complete (SC) medium containing 2% raffinose (RAF) at 30°C. Yeast cultures were diluted at $OD_{600} = 0.2$ and SiR-HALO dye was added to a final concentration of 400 nM. One hour following SiR-HALO dye addition, 10 μg/ml α-factor was added to arrest the cells in G1 phase, and the cultures were incubated for two additional hours. Cells were then immobilized on microscopy slide chambers (Ibidi) coated with 2 mg/ml concanavalin A and washed thoroughly from α-factor and SiR-HALO dye with warm SC medium containing 2% RAF prior to microscopy experiments. For the induction of *PP7-GAL10* transcription, 2% galactose (GAL) was added to the culture media 2 h before and during the microscope experiment. For hydroxyurea (HU) experiments, yeast cultures were incubated with 10 mM HU 1 h before and during the imaging. For cells with *SMC1*-AID, 1 mM of indole-3-acetic acid (IAA) was added to cells 1 h before and during the experiment. Live-cell imaging of the cells was performed on an AxioObserver inverted wide-field microscope (Zeiss) with a Colibri 7 LED light source, at 1 min intervals for 4 h at 30°C, using a x63 oil objective (NA = 1.4) in 3D (8 z-sections 0.8 μm apart). LacI-Halo-SiR and TetR-tdTomato were excited with 650 and 561 nm illumination,

respectively. PCP-Envy was excited with 488 nm illumination.

Single-molecule FISH

smFISH experiments were performed as described previously (23,24). Briefly, yeast cultures were grown in SC 2% RAF until $OD_{600} = 0.3$. Then, 2% GAL was added in the culture media and they were synchronized at G1 using 10 μg/ml α-factor for 2 h and until $OD_{600} \sim 0.5$. Next, cells were washed twice and resuspended with SC 2% RAF + 2% GAL followed by incubation for 35 min in order to enrich the population of cells in S phase. Subsequently, cells were fixed with paraformaldehyde (PFA), washed with Buffer A (1.2 M sorbitol and 100 mM potassium phosphate buffer pH 7.5), permeabilized with lyticase and washed with Buffer A. Cells were then immobilized on coverslips coated with poly-L-lysine and permeabilized with ethanol overnight. The coverslips were hybridized for 4 h with buffer containing four PP7 probes labeled with Cy5 (IDT). Finally, cells were washed with Washing Buffer (2xSSC and 10% formamide). Coverslips were mounted on glass microscope slides with anti-fading mounting media containing DAPI. Cy5 and DAPI were excited with 650 and 353 nm led illumination, respectively. Fixed cells were imaged on an AxioObserver inverted wide-field microscope (Zeiss), with Colibri 7 LED source. Transcription spots were identified using custom made Python software by fitting to a Gaussian mask including background subtraction as previously described in detail (24). The cell and nuclear borders were defined with Cell Profiler (25). Transcription sites were identified and normalized to the median fluorescent intensity of RNAs in the cytoplasm. Violin plots were plotted using the Seaborn package in Python.

Western blot analysis

For the detection of Smc1-AID-6xFLAG by western blot, 50 ml of yeast cells were grown until late-exponential phase. Smc1 depletion was induced by the addition of 1 mM of indole-3-acetic acid (IAA) for 1 h before harvest. Cells were centrifuged and pellets were frozen at −80°C overnight. Next, cell pellets were thawed and incubated in 1 ml of 0.2 M NaOH for 5 min, followed by boiling at 95°C for 5 min in 50 μl of Laemmli Buffer including 10% β-mercaptoethanol. Lysates were centrifuged for 2 min and 10 μl of the supernatants were loaded and run on a 10% SDS-PAGE gel. Separated protein bands were transferred to a PVDF membrane followed by blocking with PBST + 10% skim milk for 1 h. The membrane was washed with PBST once for 5 min, and was incubated with a primary mouse anti-FLAG antibody conjugated with HRP enzyme (1:1000) in PBST + 10% skim milk for 1 h. The membrane was washed three times with PBST and Smc1-AID-6xFLAG was detected with the EZ-ECL Chemiluminescence detection kit (Biological Industries) according to the manufacturer's protocol. Detection of Pgk1 bands was performed with a primary mouse anti-Pgk1 antibody (1:5000) and a secondary goat-anti-mouse antibody (1:10 000) conjugated with HRP.

Rad52 foci analysis

Rad52 was labeled at the C terminus with Envy by using a flexible linker, after deleting PCP-Envy from the original strains. Cell cultures were grown overnight in 2% RAF until log-phase. Then, cells were diluted in $OD_{600} = 0.15$ and were incubated for two additional hours. In induced experiments, 2% GAL was added in the media. Cells were transferred inside microscope slides and were imaged on an AxioObserver inverted wide-field microscope (Zeiss), with Colibri 7 LED source. Rad52-Envy and TetR-tdTomato were excited with 488 and 561 nm illumination, respectively. At least 280 cells were analyzed for each strain in triplicates and scored for the presence of one or more Rad52 foci. The percentage of cells with Rad52 foci was estimated by dividing the number of cells exhibiting one or more Rad52 foci by the total amount of cells at S-G2 phase. Colocalizing foci were defined as Rad52 foci which overlapped with the TetR-tdTomato foci.

HU drop assay analysis

Overnight yeast cultures were diluted at $OD_{600} = 0.2$ in YP RAF 2% and were grown for three additional hours. Cell solutions were diluted to $OD_{600} = 0.3$ and 4 μl were transferred in agar plates containing 2% RAF in the presence or absence of 2% GAL, with or without 100 mM HU, in 10-fold serial dilutions. Plates were photographed after 48 or 72 h.

RNA extraction, cDNA synthesis and quantitative RT-PCR

Yeast cells were grown to $OD_{600} = 1$ and 5 ml were harvested and centrifuged for 5 min. For the induction of PP7-*GAL10*, cells were incubated with 2% GAL for 2 h. Total RNA was isolated with the RNeasy Kit (QIAGEN) according to the manufacturer's protocol. Purified RNA samples were incubated with DNase for the removal of DNA. cDNA was synthesized with the Superscript IV First-Strand Synthesis System according to the protocol, with poly-dT primers. Quantification of PP7-*GAL10* and flanking genome transcription levels with or without galactose was conducted with quantitative RT-PCR using the *Power*SYBR Green PCR Master Mix (Thermo) according to the manufacturer's protocol. Reactions were conducted with 3.3 ng of cDNA template in triplicates for each combination of strain/set of primers. Actin (ACT1) gene was used as internal control using previously described primers (26). The sequences of primers used for qRT-PCR are shown in Supplementary Table S2. PP7-GAL10 FRW primer was designed to bind a unique sequence between the 14xPP7 repeats and the *GAL10* ORF so that only the cDNA of PP7-*GAL10* construct will be detected with the combination of PP7-GAL10 FRW and GAL10orf REV primers pair.

Quantification and statistical analysis

Time-lapse measurements were collected with ZEN 3.0 and analyzed using a custom-made computational pipeline developed specifically for the analysis of replication rates and transcription dynamics during replisome progression by our group. Our MATLAB-based pipeline identifies,

tracks and quantifies the LacI-Halo-SiR, TetR-tdTomato and PCP-Envy dots in each cell. Proper identification of the PCP-Envy dot that corresponds to the transcription site is validated by ensuring colocalization with the LacI-Halo-SiR and TetR-tdTomato dots, and the PCP-Envy background signal is subtracted to quantify transcription site intensity. Quantification results for multiple cells in each strain are averaged, while normalizing the time axis for each individual cell according to its replication rate, such that the average transcriptional intensity is calculated relative to the location of the replisome along the chromosome. Statistical analysis of replication time data and single-cell transcription intensities was performed using Monte Carlo resampling with 1 000 000 iterations (27). Pearson correlation plots were plotted, and their statistical significance was tested, using MATLAB. Swarm plots were plotted using the Seaborn package in Python.

In *SMC1*-AID strains, cells with sister-chromatid cohesion loss after replication were identified by the separation of the two copies of LacI-Halo-SiR and tetR-tdTomato dots. Subsequently, these cells were tracked after the sister-chromatid separation and the number of transcription bursts (0, 1 or 2) was manually determined at each time point.

RESULTS

Simultaneous monitoring of replisome progression and transcription dynamics at an inducible TRC

Our approach for monitoring an inducible conflict between a single replisome traveling in a known direction and a strongly transcribed gene is based on a combination of previously described systems for measuring replisome progression (27–29) and transcription dynamics (23,30) using live-cell imaging (Figure 1A,B).

Replication is monitored in real-time using arrays of bacterial operator sequences (*lacO* and *tetO*), bound by the cognate repressor fused to a fluorescent protein (lacI-HaloTag labeled with Si-Rhodamine-halo dye (lacI-Halo-SiR) and tetR-tdTomato, respectively), which allow visualization of specific chromosomal loci as fluorescent dots (Figure 1C). The timing at which each of these arrays is replicated can be monitored, as array duplication leads to recruitment of additional fluorescently labeled repressor proteins, resulting in an increase in fluorescent dot intensities (Figure 1B) (27). The *lacO* and *tetO* arrays were integrated ∼30 kb apart, within a single replicon, adjacent to an early-firing origin of replication. By measuring the time difference between duplication of the two arrays (ΔT, Figure 1B), the rate of replisome progression along the replicon can be calculated, and any significant replication fork stalling or slowdown that occurs between the arrays can be detected (27).

To generate a robust transcriptional obstacle in the path of the replisome, we integrated the *GAL10* gene, under the control of a short proximal *GAL10* promoter (31) between the *lacO* and *tetO* arrays (Figure 1A). This promoter facilitates strong unidirectional transcription of the *GAL10* gene in the presence of galactose (31). The gene was integrated in both orientations relative to the direction of replisome progression, promoting either CoD or HO collisions. In order to monitor *GAL10* transcription in real-time, 14 repeats of the PP7 stem-loop sequence were introduced within the 5′-UTR of *GAL10*. Upon PP7-*GAL10* transcription, these sequences form stem-loops within the nascent transcript, which are bound by the PP7 bacteriophage coat protein fused to the GFP Envy fluorescent protein (32) (PCP-Envy, Figure 1A). The presence of multiple PP7 loops in *GAL10* RNA at the transcription site allows visualization of this site as a fluorescent dot (Figure 1C). Quantifying the intensity of this dot over time provides a direct measure of transcriptional activity of the *GAL10* gene (30).

During live-cell imaging of cells containing these constructs in either CoD or HO orientation, a single bright PCP-Envy dot was observed in each cell during transcription bursts (Supplementary Movies S1–4) upon *GAL10* induction. This dot colocalized with the lacI-Halo-SiR and tetR-tdTomato dots (Figure 1C and Supplementary Figure S1A), confirming that it corresponds to nascent RNAs at the transcription site. All three fluorescent dots were quantified over time in yeast cells that were released into S-phase in the presence of galactose, and the relative fluorescent intensities were averaged across a cohort of cells. Assuming that an individual replisome progresses at a roughly constant rate, the replisome's position along the replicon at any point in time can be estimated, using the duplication of the two arrays as reference points (Figure 1B). However, as replisome progression rates differ between cells, we first normalized the time axis of each individual cell according to the duplication times of the arrays, and then normalized and averaged dot intensities across cells. This aligns replisome position along the replicon in all cells and allows a population-level examination of transcription dynamics during replisome progression (see below).

Replisome progression during transcription-replication encounters

To examine whether replisome progression is affected by conflicts with an actively transcribing gene, we measured the time required to replicate the span between the midpoints of the *lacO* and *tetO* arrays in individual cells, in the presence or absence of *GAL10* transcription. Surprisingly, despite the high potential for conflict due to the strength of the *GAL10* promoter, we found no significant difference in the median replication time between induced and uninduced conditions, in both CoD and HO orientations (Figure 2A). This does not depend on the specific location of the transcribed gene, as similar results were seen when the *GAL10* cassette was moved to a more origin proximal location, ∼17 kb away (Figure 2B), or even to the unrelated *URA3* locus (Supplementary Figure S1B,C). These findings demonstrate that replisome progression is robust in the face of transcription in either CoD or HO orientation and highlight the efficient coordination between the replication and transcription machinery that prevents detrimental TRCs.

Since TRCs can lead to genomic instability, we examined whether *GAL10* induction in our strains causes increased sensitivity to hydroxyurea (HU), which may indicate the presence of DNA damage (Supplementary Figure S2). We
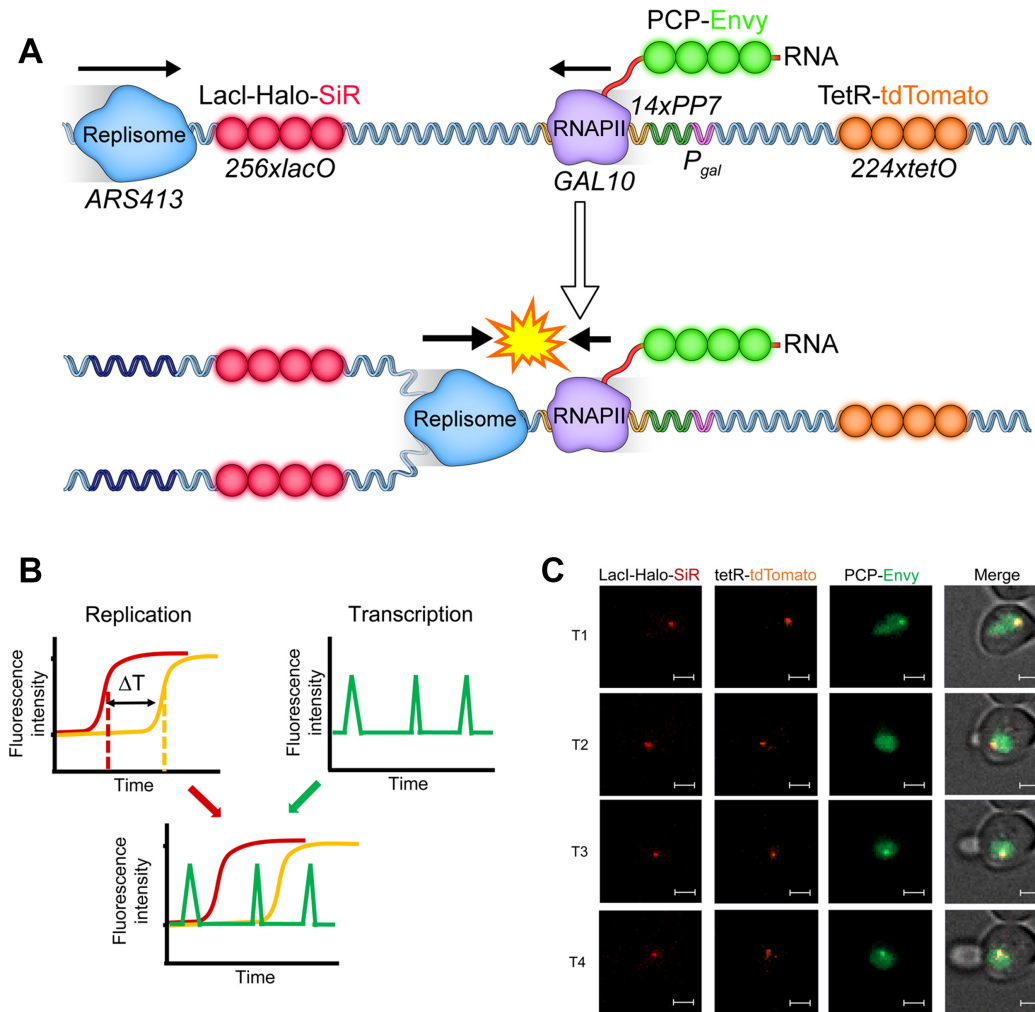
Figure 1. Real-time monitoring of replisome progression and transcription dynamics at the same locus in single live cells. (**A** and **B**) Schematic illustration of the experimental system. Replisome progression is monitored using two bacterial operator arrays, 256x*lacO* and 224x*tetO*, integrated downstream of an active and isolated origin of replication (*ARS413*) and labeled by LacI-Halo-SiR and TetR-tdTomato. For simplicity, only replisome progression toward the arrays is shown. During DNA replication, duplication of the operator arrays leads to the recruitment of additional fluorescently labeled repressors, resulting in an increase in fluorescence intensity (**B,** top left). The difference between the midpoint increases in fluorescence due to *lacO* and *tetO* array duplication (ΔT) is an indicator of the time required to replicate the mid-array distance. Transcription is monitored using *GAL10* containing 14xPP7 repeats at the 5′ UTR, integrated between the two arrays (only HO orientation is shown here (A)). Binding of PCP-Envy to PP7-*GAL10* transcripts allows the live-cell detection of transcription bursts during DNA replication and cell cycle progression (**B,** top right). Real-time monitoring of replisome progression and transcription dynamics is enabled by the simultaneous measurements of replication and transcription fluorescent signals (**B,** bottom). (**C**) Representative cell with labeled *lacO* and *tetO* arrays visible as LacI-Halo-SiR and TetR-tdTomato dots. Transcription bursts are visible as PCP-Envy dots that colocalize with the labeled arrays; scale bar is 2 μm.

found no change in HU sensitivity (Supplementary Figure S2A), consistent with the absence of fork stalling. Furthermore, while our system can detect double strand breaks (DSB) between the *lacO* and *tetO* arrays (Supplementary Figure S3), we did not observe DSBs in any of the induced cells, nor did we detect an increase in the number of Rad52 foci, a marker for DSB repair (33), upon *GAL10* induction (Supplementary Figure S2B). These results suggest that TRC-induced fork stalling that is sufficiently severe to create DSBs is a relatively rare occurrence.

Dynamics of *GAL10* transcription prior, during and following gene replication

To examine how the robustness of replisome progression relates to the level of transcriptional activity, we measured

GAL10 transcription dynamics using live cell imaging in the above strains during replisome progression and duplication of *GAL10* (Figure 3A). In cells containing *GAL10* in a CoD orientation, alignment of transcription intensities with the timings of *lacO* and *tetO* array replication revealed three distinct phases with differing *GAL10* transcription levels (L1–L3, Figure 3B and Supplementary Figure S4). During replisome progression, transcription levels decrease significantly between the L1 and L2 phases and recover at L3. The transition to the lower transcription level seen at L2 begins in early S-phase, just as the first array is being replicated, and the recovery to L3 occurs rapidly, just after the *GAL10* gene has been replicated (Figure 3B). This indicates that transcription is not only repressed during replication of the transcribed gene, but repression starts long before the replisome reaches the actual gene.
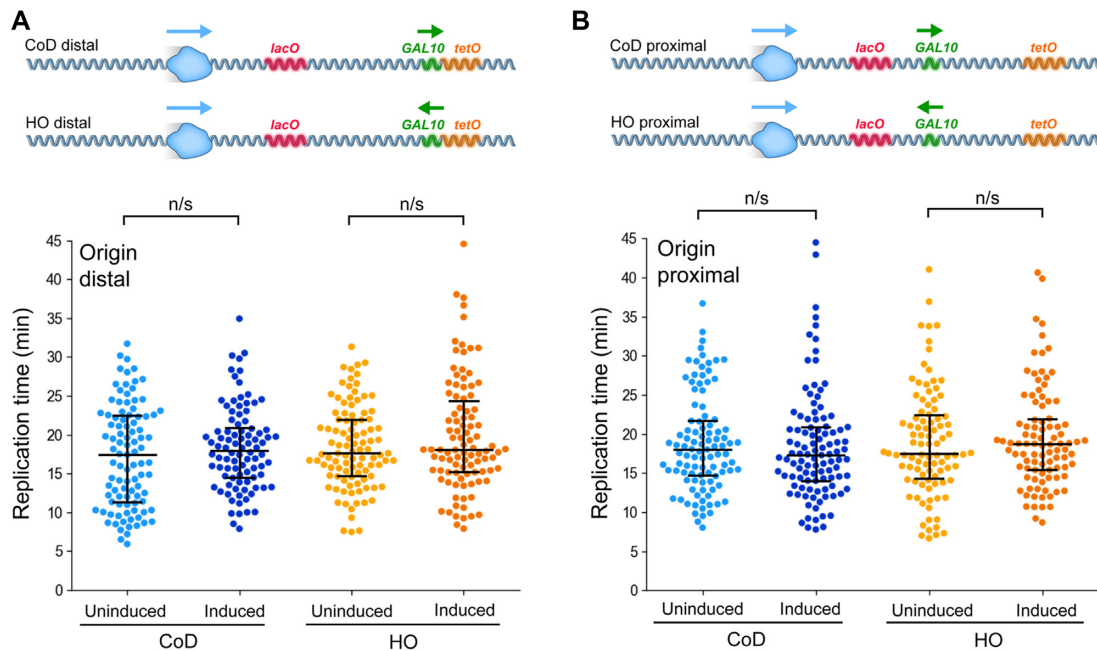
Figure 2. Replication fork progression measured in the presence or absence of *GAL10* transcription. (**A**) Top: Schematic representation of DNA replication from *ARS413* (blue) through *GAL10* (green) located at an origin-distal location, in CoD and HO orientations relative to fork progression. Bottom: Replication times in origin-distal CoD (blue) and HO (orange) cells, in either the absence (uninduced, 97 cells for CoD and 100 cells for HO) or presence (induced, 92 cells for CoD and 98 cells for HO) of *GAL10* transcription. (**B**) Same as (A) but for *GAL10* located at an origin-proximal location in either the absence (uninduced, 101 cells for CoD and 94 cells for HO) or presence (induced, 105 cells for CoD and 95 cells for HO) of *GAL10* transcription.

To identify the timing of transcription repression and recovery relative to *GAL10* replication, we fitted sigmoidal functions to the averaged transcription profiles and calculated the midpoint of each phase transition (Figure 3B). Assuming a constant replisome progression rate, the difference between the timing of transcriptional repression (L1 to L2 transition) and *GAL10* replication can be translated to a distance of ∼27 kb in the CoD cells, meaning that *GAL10* transcription is repressed when the replisome is ∼27 kb upstream from *GAL10* (Table 1). In contrast, the distance between *GAL10* and the transcription recovery midpoint (L2 to L3 transition) is only ∼4 kb downstream from *GAL10*, indicating fast recovery of *GAL10* transcription following gene replication.

To examine whether the observed transcriptional changes occur at fixed times or are correlated to replisome progression toward the transcribed gene, we analyzed transcription in cells containing the *GAL10* cassette at a different location between the *lacO* and *tetO* arrays, ∼17 kb closer to the origin (Figure 3C). We found that the overall pattern of 3-phase transcription dynamics was similar to that seen in the previous location, but the repression of transcription (L1 to L2 transition) and its recovery occurred much earlier (Figure 3C and Supplementary Figure S4). The shifts in repression and recovery timings were roughly proportional to the shift in *GAL10* location, occurring when the replisome appears to be >30 kb upstream and ∼4 kb downstream from *GAL10*, respectively (Table 1). In practice, since *GAL10* is located just ∼22 kb from the adjacent origin (*ARS413*) in this strain (Figure 3C), this observation suggests that transcriptional repression takes place approximately with origin firing. Taken together, these results demonstrate that tran-

scription is partially repressed well before the replication fork reaches the transcribed gene, and that this repression depends on the location of the replisome relative to the transcribed gene, rather than being a global decrease of transcription levels during S-phase.

To further validate that replisome progression is indeed responsible for the patterns of *GAL10* transcription observed during S-phase, we examined transcription in cells containing the *GAL10* cassette at the *URA3* locus on chromosome V rather than between the *lacO* and *tetO* arrays. In this strain, replisome progression from *ARS413* should have no effect on *GAL10* transcription. Indeed, we found no evidence of the 3-phase transcriptional pattern seen in the other strains (Figure 3D) and observed no colocalization between the PCP-Envy dot and the lacI-Halo-SiR and tetR-tdTomato dots as expected (Supplementary Figure S1C).

In a strain harboring a HO conflict, we found that repression of *GAL10* transcription ahead of the fork takes place in two phases, the L1 to L2 transition taking place at a similar timing as the respective CoD strain and L2 to L3 transition taking place much closer to the *GAL10* gene. The degree of transcriptional repression of L3 appeared to be greater than in the CoD strains (Figure 3E and Supplementary Figure S4). This might suggest that in the case of a HO conflict, which is more severe than a CoD conflict (7,8), unhindered replisome progression comes at a cost of lower transcription during replication. A strain with a HO *GAL10* at the more origin-proximal location showed a somewhat different pattern, with early decrease of transcription, similar to the CoD orientation at the same location, and slower recovery after *GAL10* replication (Figure 3F). Such differences may
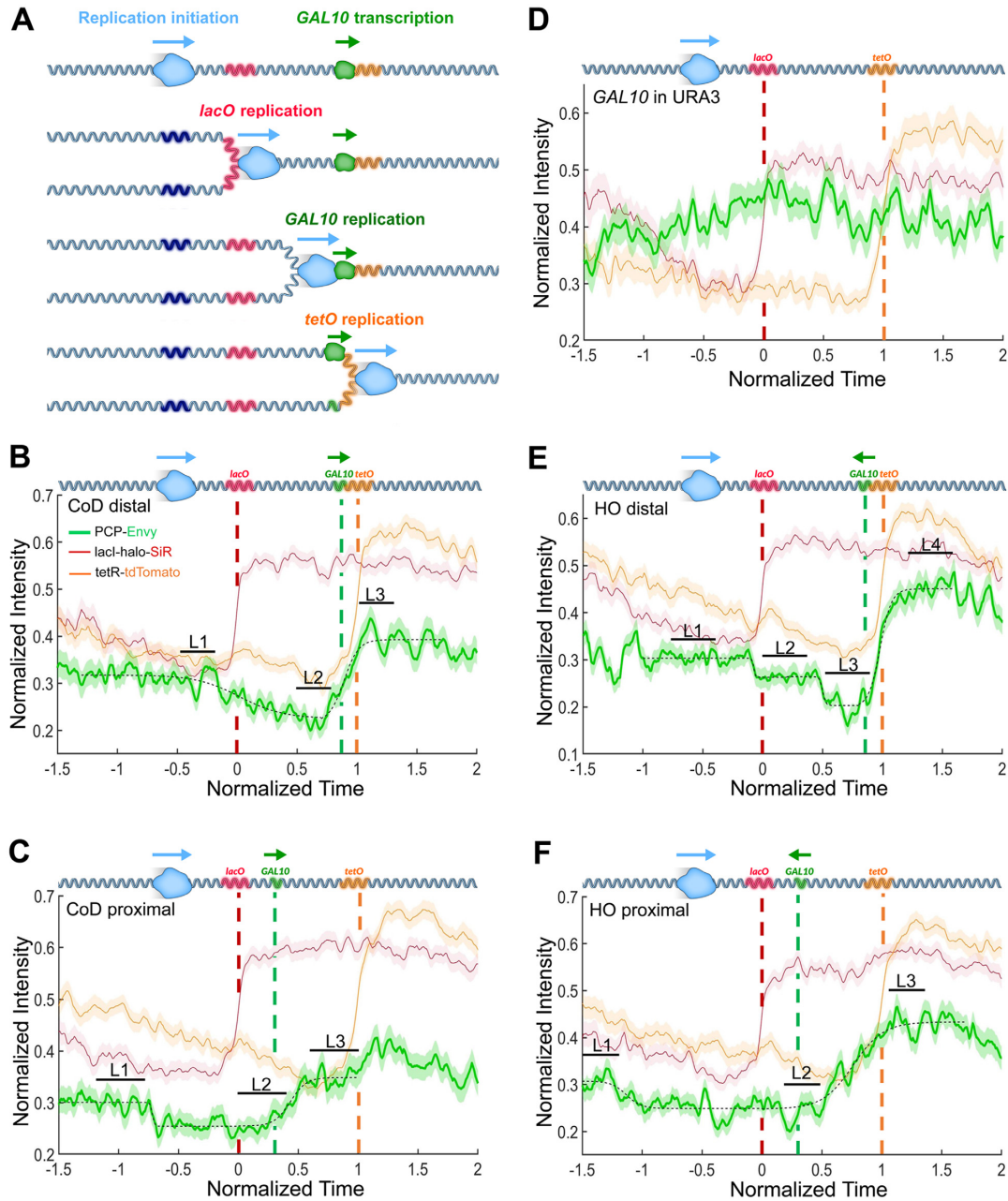
Figure 3. *GAL10* transcription dynamics during replisome progression. (**A**) Schematic representation of replisome progression from *ARS413* during *GAL10* transcription. (**B**) Normalized fluorescent intensity of the transcription site (PCP-Envy dot) as well as the *lacO* and *tetO* arrays (lacI-Halo-SiR and tetR-tdTomato dots, respectively), averaged over 87 cells from a strain with *GAL10* in a CoD orientation. The time axis is normalized according to the duplication times of the arrays. Shaded areas represent standard error of the mean. Dashed vertical lines represent the duplication times of the two arrays and the *GAL10* gene. Dashed black lines represent a fit of the transcription intensity data to a sigmoidal function (see Table 1 for the distance between the phase transition midpoints and the *GAL10* gene). The average transcription levels within the labeled L1, L2 and L3 time windows (see Supplementary Table S1 for the extent of each time window) are significantly different from each other (see Supplementary Figure S4). (**C**) Similar to (**B**) but for 97 cells containing *GAL10* in a CoD orientation in an origin-proximal location. (**D**) Similar to (**B**) but for 56 cells containing *GAL10* at the *URA3* locus, rather than between the *lacO* and *tetO* arrays, such that transcription levels do not correspond to replisome location in the *ARS413*-adjacent replicon. (**E** and **F**) similar to (**B**) but for cells containing *GAL10* in a HO orientation, in an origin-distal (**E**, 89 cells) or origin-proximal (**F**, 90 cells) location.

Table 1. Distance of *GAL10* transcription repression or recovery from the *GAL10* gene

Strain	Distance of *GAL10* transcription repression ahead of the replisome (kb)	Distance of *GAL10* transcription recovery following *GAL10* duplication (kb)
CoD distal	27.1	3.9
HO distal	30.3/10.0[c]	7.1
CoD proximal	>22[b]	4.4
HO proximal	>22[b]	16.1
rpb1-1 CoD[a]	14.9	3.0
rpb1-1 HO[a]	>22[b]/5.6[c]	13.3
rpb1-1 HO fast[a]	>22[b]	15.4
rpb1-1 HO slow[a]	5.6[c]	13.7
HO 10 mM HU[a]	>22[b]	11.3
top1Δ CoD[a]	>22[b]	12.6
top1Δ HO[a]	>22[b]/3.2[c]	-

[a]Strains containing *GAL10* in a proximal CoD or HO orientation.
[b]Suppression of *GAL10* takes place upon or before replication initiation from *ARS413* which is located 22 kb away from *GAL10*.
[c]Second phase of repression taking place at the region of *GAL10* gene.

be related to the specific chromosomal environment of the transcribed gene.

Overall, these results demonstrate that replisome progression is associated with a significant long-range decrease of transcription downstream from the fork, and hint at the possibility of a 'wave' of transcriptional repression traveling ahead of the replisome as it progresses. This repression may reduce the probability of harmful collisions between the replication and transcription machinery and facilitate smooth replisome progression through highly transcribed regions. Notably, transcription is only partially repressed during replication, highlighting the efficient coordination between the two processes which enables their coexistence during gene replication. Following replication of the transcribed gene, transcription levels recover quickly, highlighting the efficiency of replication-coupled chromatin assembly for promoting transcription (34).

Correlations between fork progression and transcriptional activity indicate efficient transcription-replication coordination

To study the relationship between fork progression and transcriptional activity at the single-cell level, we calculated the degree of transcriptional repression for each cell by comparing the average *GAL10* transcription levels within various time windows before and during the repression phases (Figure 3 and Supplementary Figure S4, Supplementary Table S1). We found a significant intra-population correlation between the degree of transcriptional repression in each cell and its replication time (Supplementary Figure S5). This correlation was positive, indicating that when a highly transcribed gene is present in the path of the replisome, cells with slower replisome progression tend to also have deeper repression of transcription while the gene is being replicated. This result demonstrates that high transcriptional activity does not come at the expense of replisome progression in WT cells and highlights that proper coordination of replication and transcription is important for both processes to proceed normally.

Overall transcription levels are not affected by *GAL10* directionality

While our live-cell imaging approach allows high-resolution monitoring of *GAL10* transcription during replication, the absolute number of nascent RNA molecules at the transcription site is difficult to measure accurately. To examine whether differences in replication and transcription dynamics between the CoD and HO strains stem from variations in absolute transcription levels, we used single-molecule RNA fluorescence *in situ* hybridization (smFISH) (35,36) and verified that transcription site foci colocalizes with the fluorescently labeled array dot (Supplementary Figure S6A). This approach allows measuring the number of nascent RNAs at the transcription site and was previously used to analyse transcription sites in the natural *GAL10* locus (30). Using smFISH on mid S-phase cells, we found a very similar number of RNAs per transcription site in CoD and HO cells (Supplementary Figure S6), indicating no significant effect of *GAL10* orientation on overall transcription levels during S-phase. Additionally, we measured transcription using qRT-PCR at and around the *GAL10* gene under induced and uninduced conditions. This further verified the similar transcription levels of CoD and HO strains and validated that *GAL10* transcription is unidirectional and does not extend beyond the gene itself (Supplementary Figure S7).

Simultaneous transcription from both *GAL10* copies following gene replication

During S-phase, gene expression was shown to be buffered against changes in gene dosage due to genome duplication (2). Nevertheless, in the case of *GAL10* we noted that transcription levels after gene duplication were somewhat higher than those seen in late-G1/early-S phase, particularly in HO strains (compare L1 and L3, Figure 3 and Supplementary Figure S4). We wondered whether the increased transcription following gene duplication is due to higher transcription activity on one of the copies of *GAL10*, or whether transcription can take place simultaneously from both gene copies. However, our ability to determine whether transcription takes place on one or two gene copies during late-S/G2 is hindered by sister chromatid cohesion, which ensures colocalization of the two copies. To overcome this difficulty, we abolished cohesion by depleting Smc1 using the auxin-inducible degron (AID) system following release of cells into S-phase (Supplementary Figure S8) (20,37). In the absence of cohesion, the fluorescent dots on each of the chromatids should visibly separate soon after DNA replication (27), allowing the detection of transcription from each *GAL10* gene copy separately. Indeed, we found that Smc1 depletion in CoD and HO cells results in early separation of the lacI-Halo-SiR and tetR-tdTomato dots following array duplication (Figure 4A). Remarkably, we were able to detect transcription bursts from both *GAL10* copies following gene replication (Figure 4A). Systematic analysis of *GAL10* transcription events revealed high frequency of transcription from both gene copies (Figure 4B). These results demonstrate that the two gene copies can be transcriptionally active following gene duplication, and efficient transcription can take place simultaneously from these copies.

A

Transcription during G2 in Smc1-depleted cells
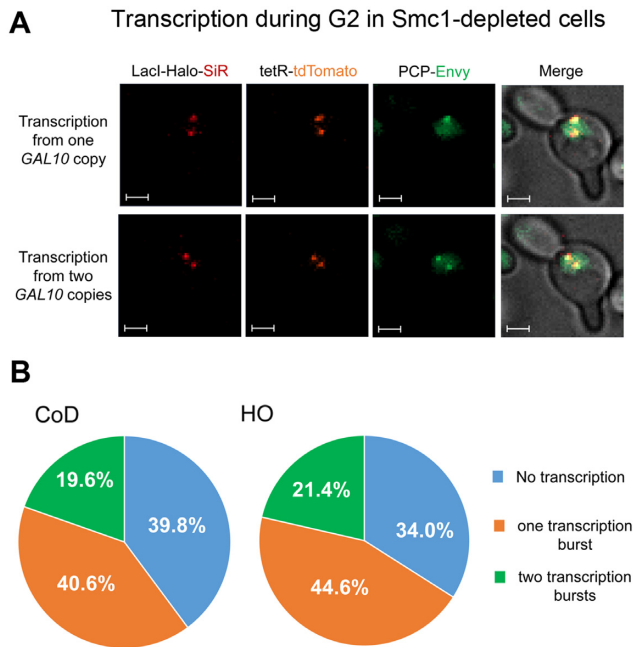
Figure 4. Simultaneous transcription from the two *GAL10* gene copies following gene replication. Transcription was measured in the absence of cohesion (Smc1-AID) to detect *GAL10* transcription from the two sister chromatids following gene replication. (**A**) Images of representative yeast cells at G2 containing *GAL10* at the CoD orientation in the absence of cohesion. Sister chromatid separation is monitored by the appearance of two dots of TetR-tdTomato and LacI-Halo-SiR during G2 phase (left). One or two dots of PCP-Envy (middle) that colocalize with the replication dots (right) show transcription from one or two copies of *GAL10*, respectively; scale bar is 2 μm. (**B**) Percentage of time points where 0, 1 or 2 *GAL10* transcription dots are detected out of 2688 and 1897 observations from 40 CoD and 30 HO cells, respectively.

Accumulation of RNAPII impairs replication-transcription coordination

Our results suggest that transcription of the *GAL10* gene is repressed prior to its replication, and this effect may be related to efficient replication-transcription coordination. To examine whether proper eviction of RNA polymerases from the transcribed gene facilitates this coordination, we employed our approach to examine the *rpb1-1* mutant, which was previously shown to have increased retention of RNAPII on chromatin (10). In accordance with a previous study (10), we found that replication is significantly slower in *rpb1-1* cells upon induction of *GAL10* transcription in both CoD and HO orientations (Figure 5A).

Analysis of transcription dynamics in *rpb1-1* cells with CoD *GAL10* transcription during replisome progression showed a similar pattern to WT cells, with a minor delay in the appearance of transcriptional repression ahead of the replisome (Supplementary Figure S9AB and Table 1). Interestingly, analysis of *GAL10* transcription dynamics in *rpb1-1* HO cells, revealed a pattern with 4 phases, instead of the 3 seen in the corresponding WT strain (comparison of Figure 5B and Figure 3F). The repression of transcription appeared to take place in two stages: the L1 to L2 transition, when the replisome is ∼22 kb ahead of *GAL10*, and the L2 to L3 transition which occurred just ∼6 kb ahead of *GAL10*

(Figure 5B, Supplementary Figure S9C and Table 1). We examined the transcription dynamics of the fast-replicating cells, which exhibit shorter than median replication times and observed a single transcriptional repression phase beginning ∼22 kb ahead of *GAL10* (Figure 5C and Supplementary Figure S9D). In contrast, examining the transcription dynamics of the complementary slow-replicating cells showed a relatively strong transcriptional repression occurring relatively late, just before *GAL10* replication (Figure 5D and Supplementary Figure S9E). In addition, we found a significant positive intra-population correlation between the degree of transcriptional repression and replication time within the *rpb1-1* HO and CoD populations (Supplementary Figure S10AB). Overall, these results indicate that the *rpb1-1* mutation impairs the coordination between replication and transcription at least in some of the cells, leading to both longer replication times, indicative of fork stalling or slowdown and deeper repression of transcription in those cells. However, we did not detect DSBs between the *lacO* and *tetO* arrays in any of the *rpb1-1* cells nor increased levels of Rad52 foci (Supplementary Figures S2 and S3).

To verify that the pattern of transcriptional repression, observed in the slow *rpb1-1* cell population (Figure 5D), is not just a byproduct of slower replisome progression but a result of transcription replication encounters, we examined transcription dynamics in WT HO cells exposed to 10 mM hydroxyurea (HU). We found that exposure to HU does not affect transcription dynamics despite a very significant slowdown in replisome progression (Supplementary Figure S10CD), highlighting the effect of fork stalling or slowdown as a result of the *rpb1-1* mutant. Finally, to examine whether the observed behavior of the *rpb1-1* mutant is correlated with an increase in absolute transcript numbers at the transcription site, we analyzed the *rpb1-1* CoD and HO strain using smFISH. We found no significant change in RNA levels at the transcription site (Supplementary Figure S10E), further supporting that the presence of the RNAPII complex, rather than overall transcription levels, is the source of the TRCs observed in the mutant cells.

Overall, these results suggest that efficient coordination between the replication and transcription machinery requires proper removal of the RNAPII complex from the chromatin (10). Potentially harmful collisions caused by the accumulation of RNAPII not only stall replication forks but also decrease transcription levels during replication of the transcribed region, further highlighting the importance of proper coordination for both replisome progression and continued transcriptional activity.

Efficient coordination of replication and transcription requires topoisomerase I

During replisome progression, the unwinding of DNA generates positive supercoiling ahead of the replisome, leading to topological stress. The accumulation of such topological stress in front of the replisome must be relaxed by topoisomerases to prevent harmful TRCs, particularly when replication and transcription collide in a head-on orientation (12,38). Indeed, several studies have shown that mutations in topoisomerases can lead to replication stalling and DNA breaks at transcribed genes (11,12,39). To examine how
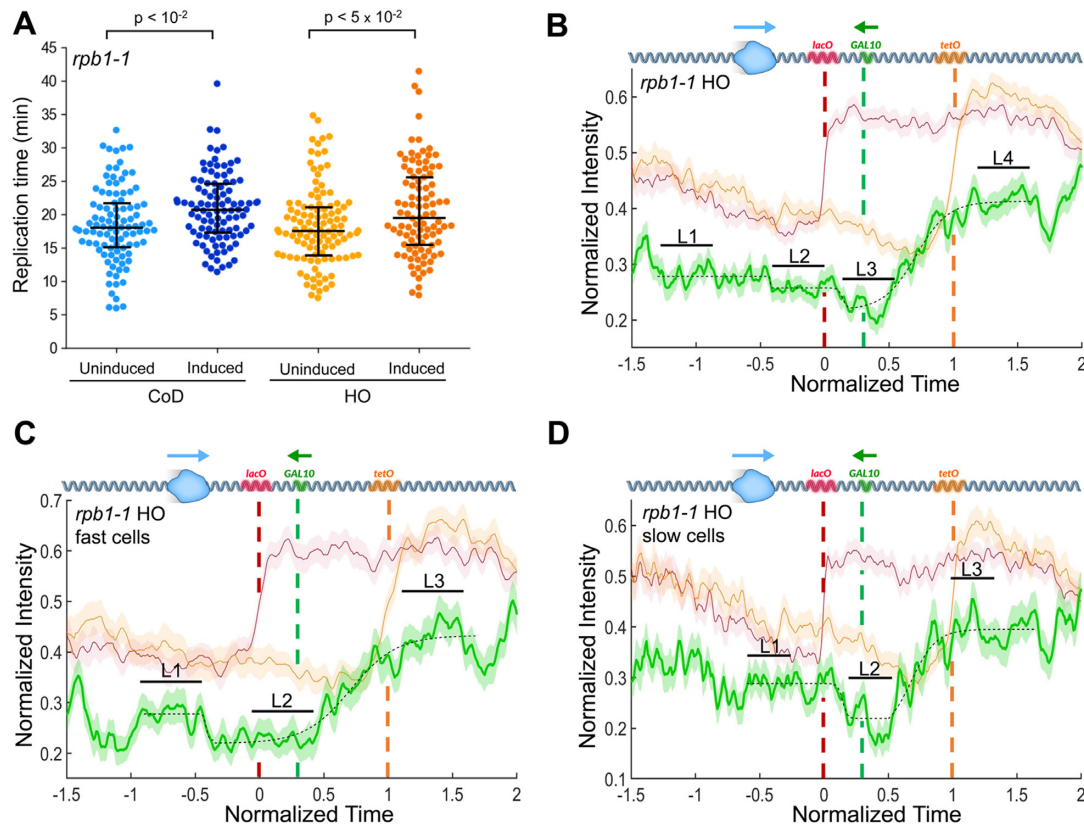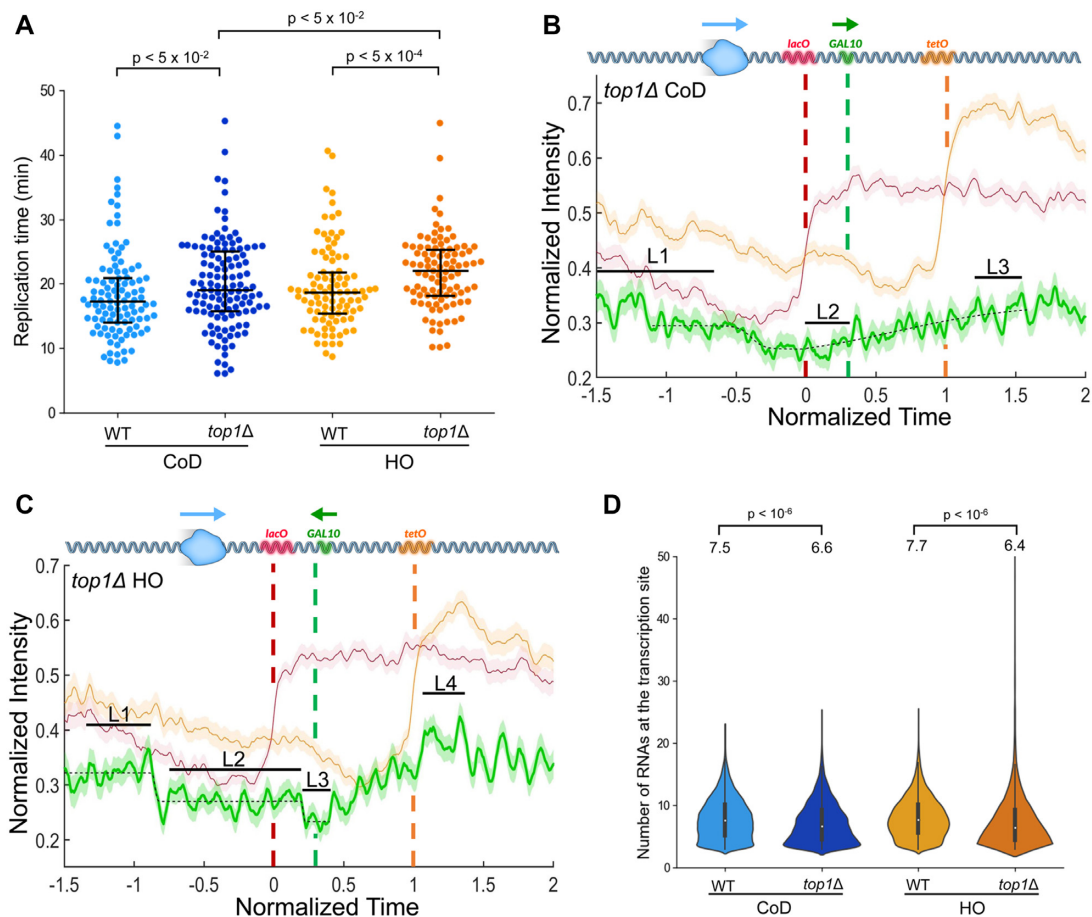
Figure 5. Replication fork progression and transcription dynamics in *rpb1-1* cells. (**A**) Replication times for *rpb1-1* CoD (blue) and HO cells (orange) measured under uninduced or induced conditions (uninduced, 98 cells for HO, induced, 100 cells for CoD and 97 cells for HO). (**B**) Normalized fluorescent intensity of the transcription site and arrays, as described in Figure 3B, averaged over 92 cells from a *rpb1-1* HO strain. (**C** and **D**) Normalized fluorescent intensity of the transcription site and arrays for a subpopulation of 45 cells that showed faster than median replication times (C) and a subpopulation of 47 cells that showed slower than median replication times (D). See Table 1 for the distance between the phase transition midpoints and the *GAL10* gene. See Supplementary Figure S9 for transcription levels within the labeled L1–L4 time windows and their statistical significance, see Supplementary Table S1 for the extent of each time window. All experiments were performed at 30°C.

topological stress affects the coordination between replication and transcription in real-time, we deleted topoisomerase I (*top1Δ*) on the background of both the CoD and HO strains.

Consistent with a previous study in mammalian cells (11), we detected significantly slower replication in *top1Δ* cells in the presence of *GAL10* transcription in both orientations, although the effect was significantly more pronounced in the HO strain (Figure 6A). Detailed analysis of the *top1Δ* HO cells revealed a significant subpopulation of cells in which no *GAL10* transcription could be detected throughout the cell cycle, despite induction by galactose. Interestingly, replication times in *top1Δ* HO transcribing cells were longer than in non-transcribing cells, indicating slower fork progression in the presence of *GAL10* transcription and topological stress (Supplementary Figure S11A). The induced WT HO strain also had a sub-population of cells with no transcription, but these cells showed no difference in replication times (Supplementary Figure S11A), consistent with the lack of effect of *GAL10* transcription on replisome progression in WT strains (Figure 2).

Next, we analyzed the transcription dynamics of *top1Δ* CoD and HO strains. We found that the transitions between phases were much more gradual in *top1Δ* CoD cells, rela-

tive to the corresponding WT strain (Figure 6B). This may indicate that the accumulation of topological stress ahead of the fork is not neutralized by the negative supercoiling behind RNAPII and still affects the downstream codirectional transcription. This result also highlights the importance of topological stress in enabling efficient transcriptional repression ahead of the fork. Additionally, complete transcriptional recovery following *GAL10* replication was dramatically delayed taking place ∼30 kb downstream of *GAL10*, suggesting that topological stress can also have significant effects on transcription behind the fork (Figure 6B, Supplementary Figure S11 and Table 1). The *top1Δ* HO strain also showed transcriptional repression similar to WT strains, except that an additional phase of stronger repression appeared, precisely overlapping with replication of *GAL10* (L3, Figure 6C and Supplementary Figure S11). These results suggest that excess topological stress due to convergent replication and transcription can lead to further dampened transcription as the replisome reaches the transcribed region. To compare absolute transcription levels, we measured the number of nascent RNA molecules at the transcription site in *top1Δ* CoD and HO strains using smFISH. We found a small decrease in the number of RNAs in *top1Δ* strains in both orientations compared to WT cells

Figure 6. Replication fork progression and transcription dynamics in *top1Δ* cells. (**A**) Replication times for *top1Δ* cells in CoD or HO orientations, the corresponding results for WT cells are shown for comparison. Significant slowdown in replication is observed for the *top1Δ* cells relative to the WT cells (105 cells for WT and 122 cells for the *top1Δ* CoD, and 95 cells for WT and 97 cells for the *top1Δ* HO). (**B** and **C**) Normalized fluorescent intensity of the transcription site and arrays, as described in Figure 3B, averaged over 99 cells from a *top1Δ* CoD strain (B) and 93 cells from a *top1Δ* HO strain (C). See Table 1 for the distance between the phase transition midpoints and the *GAL10* gene. See Supplementary Figure S11 for transcription levels within the labeled L1–L4 time windows and their statistical significance and see Supplementary Table S1 for the extent of each time window. (**D**) Number of RNAs at the transcription sites in WT and *top1Δ* cells determined using smFISH. The median values (white dots) for each strain are noted, and the boxes indicate the 25–75% percentile of the population. The number of cells analyzed is 52 472 for WT CoD, 18 094 for *top1Δ* CoD, 48 140 for WT HO and 24 682 for *top1Δ* HO strain. The corresponding results for WT cells (Supplementary Figure S6) are shown as a comparison.

(Figure 6D) in accordance with the effect of topoisomerases on transcription in yeast (40).

Overall, these results demonstrate that topological stress impairs replication-transcription coordination, leading to fork stalling or slowdown and lower transcription. Some *top1Δ* cells which maintain *GAL10* transcription, despite the topological stress, suffer from fork stalling or slowdown, while in others, in which transcription is suppressed, fork stalling is prevented. The existence of a non-transcribing *top1Δ* HO sub-population with normal replisome progression highlights the trade-off between transcription and replication in this strain and demonstrates that replication and transcription cannot properly coexist on the same template unless topological stress is relaxed.

DISCUSSION

In this study, we developed an approach for the real-time monitoring of replication and transcription at the same locus in single live yeast cells (Figure 1). This approach en-

ables high-resolution measurements of transcription during replisome progression through a transcribed gene and in parallel, measuring the effect of transcription on replisome movement. We applied this approach for measuring replication fork progression and *GAL10* transcription to reveal how these two processes are coordinated during an induced TRC. We chose to monitor *GAL10* transcription due to its high activity upon induction (30), allowing the sensitive detection of transcriptional changes during replisome progression and increasing the severity of the induced TRC. However, our system is highly modular and thus can be applied for the real-time measurement of replication and transcription of a variety of other genes at different genomic loci.

Coordination of replisome progression and transcription

The detection of transcription repression ahead of the replisome and its recovery soon after *GAL10* replication demonstrates the tight coordination between replisome progres-

sion and *GAL10* transcription during S-phase (Figures 2 and 3). The transcriptional repression, taking place ahead of the replisome, may minimize the severity of collision between the replisome and transcription machinery and prevent fork stalling. Indeed, our findings that replication fork progression is not affected by *GAL10* transcription are in accordance with this hypothesis (Figure 2). Previous genome wide studies in yeast examining fork stalling during cell cycle progression reported mixed observations. While one study detected fork stalling at highly transcribed genes (41), another study found uniform replication fork progression throughout the genome (42). Our results showing no significant fork stalling or slowdown highlight the robustness of replisome progression in the face of high levels of transcription. The fact that we observed no DSBs in any of our strains suggests that such TRCs (Supplementary Figures S2 and S3) do not commonly lead to genomic instability. DSBs may occur following more severe fork stalling that is too rare to observe using our system.

Transcription dynamics during replication fork progression

Surprisingly, we found that transcriptional repression of *GAL10* can take place up to 30 kb ahead of the replisome (Figure 3 and Table 1). Previously, it was discovered that a wave of histone modifications propagates several kilobases ahead of the moving replisome, promoting gene expression homeostasis (43). Thus, it is possible that transcriptional repression, measured in our experiments, is mediated by a wave of chromatin modifications moving ahead of the replisome. However, further studies are needed to explore the nature of this phenomenon. Consistent with *GAL10* repression ahead of the replisome, recent studies have shown that transcription factors are evicted from promoters during early DNA replication in yeast (44), and transcription is reduced during early S-phase in mammalian cells (45). Transcription repression ahead of the replisome could be related to minimization of TRCs to prevent harmful collisions between the machinery. The finding that slower replisome progression is associated with deeper repression of transcription during replication of the transcribed gene (Supplementary Figure S5) indicates that efficient coordination enables fast replisome progression concomitant with continued transcription. Thus, not only is replisome progression unhindered by active transcription in WT cells (Figure 2), but fast replication is conducive to increased transcriptional activity in the path of the replisome. It is possible that the transcriptional repression that we observed ahead of the replication fork, prevents even deeper repression during *GAL10* replication.

Our observation of fast transcriptional recovery following *GAL10* replication (Figure 3) is in accordance with studies in yeast showing that transcriptional recovery occurs minutes following gene replication and assists chromatin formation (34). Our results showing high frequency of simultaneous transcription from both *GAL10* copies in cohesion-depleted cells (Figure 4) suggest that buffering of gene expression following replication does not take place by restricting access of RNAPII to one of the two *GAL10* gene copies but can be mediated by reducing transcription intensity of each copy during G2 (2).

TRCs exacerbated by RNAPII accumulation on chromatin

While our measurements in WT cells highlight the characteristics of efficient replication-transcription coordination, the examination of *rpb1-1* cells revealed TRC-associated replication fork stalling or slowdown as well as decreased transcription during replication of the transcribed gene (Figure 5). Previously, it was shown that RNAPII itself can serve as a roadblock for replisome progression during transcription in bacteria (46,47) and in yeast (10). Specifically, previous analysis of *rpb1-1* revealed genome wide defects in replisome progression, alteration in transcription and increased levels of site-specific recombination (10). The examination of *rpb1-1* in our system allowed the detection of different behaviors within the HO collision population: while faster replicating cells showed transcription repression a long distance ahead of the replisome, slow replicating cells were characterized by significant but late-onset transcription repression (Figure 5). These results are consistent with a scenario in which collisions of the moving replisome with RNAPII can result in replisome stalling on *GAL10* and RNAPII displacement from the DNA, preventing *GAL10* transcription. In agreement with this scenario, an *in vitro* study in a bacterial system has shown that HO collisions result in RNAP displacement from the DNA and replisome stalling (48). The absence of dramatic fork stalling indicates that after collision, the replisome stays intact and quickly resumes DNA replication, consistent with the *in vitro* study described above (48). Finally, our observation that DSBs do not occur in any of our strains including *rpb1-1* cells (Supplementary Figures S2 and S3), further supports efficient replication restart following fork stalling or slowdown.

Previous studies in WT and mutant strains, including *rpb1-1*, used genetic assays to examine the frequency of site specific recombination events due to TRCs (8,10). This approach, relying on the activation of repair pathways, allowed measuring the acute consequences of rare TRCs. In contrast, our real-time measurements of HO and *rpb1-1* cells, performed under non-selective conditions, allow the direct detection of TRCs in their common forms. The heterogeneous nature of these TRCs, with some cells experiencing more significant fork stalling or slowdown and transcriptional repression than others, suggests that the replisome can encounter different numbers and conformational states of RNAPIIs in different cells. In agreement with this possibility, it was shown that during transcription elongation, RNAPII tends to spontaneously pause at specific DNA sequences (49,50) leading to significant conformational changes in the complex (51). These conformational changes can trap RNAPII in a stable and inactive state, increasing the chances of collision with the replisome.

Trade-offs between replication and transcription in the presence of topological stress

Excess of topological stress, accumulating during replisome and RNAPII progression on the DNA, was shown to aggravate TRCs in cells, especially in the HO orientation (11,12,52). Topoisomerase I (Top1), which is localized to ORFs in yeast (53), is the enzyme that relieves positive supercoiling accumulated in front of replication forks and RNAPII (38,54). Thus, the real-time examination of *top1*Δ

cells allowed us to study the effect of increased topological stress on replication-transcription coordination. The slow-down of replisome progression in the *top1Δ* cells due to *GAL10* transcription, particularly in the HO orientation (Figure 6A), is consistent with previous reports of increased positive supercoiling accumulated in *top1Δ* HO cells (12,38) and stalled replication forks found in mammalian cells depleted of Top1 (11). Interestingly, our single cell *top1Δ* HO measurements revealed a trade-off between replication and transcription, as cells that did not transcribe showed normal replication rates (Supplementary Figure S11A). This trade-off was discovered by the identification of two *top1Δ* HO cell sub-populations with different replication times, high-lighting the importance of single cell analysis to identify distinct differences in cellular behavior within an isogenic cell population.

Finally, the dramatic delay in transcription recovery following *GAL10* replication, observed in the *top1Δ* CoD cells, is another manifestation of the altered coordination between replication and transcription in these cells (Figure 6 and Table 1). One possible explanation is that negative supercoiling behind the replisome affects transcription dynamics leading to a delayed transcription recovery. Indeed, our smFISH analysis detected reduced *GAL10* transcription in the *top1Δ* cells (Figure 6D), consistent with a previous study showing that mutations in *top1* and/or *top2* lead to reduced *GAL10* expression (40).

In summary, we developed a live-cell imaging approach for monitoring replisome progression and transcription dynamics in real-time during encounters between the replication and transcription machinery. Our experiments and analysis revealed long-range transcriptional repression ahead of the moving fork that may facilitate smooth replisome progression through the transcribed gene. In addition, we monitored conflicts taking place in real-time and found that efficient transcription-replication coordination allows both faster replisome progression and higher transcription levels. Our approach allowed the detection of unique sub-populations of cells with distinct behaviors and trade-offs between replication and transcription. This live-cell imaging system can be applied for the study of additional mechanisms for prevention of conflicts (e.g. R-loop resolution) and the examination of conflicts arising from the transcription of other genes. Overall, our study sheds new light on the coexistence of replication and transcription for maintaining genomic stability during cell growth and division.

DATA AVAILABILITY

All data and code for analysis are available upon request.

SUPPLEMENTARY DATA

Supplementary Data are available at NAR Online.

ACKNOWLEDGEMENTS

We thank Ron Milo, Yoav Voichek and Ariel Afek for advice along the project and critical reading of the manuscript. We thank Douglas Lutz for technical help with the live-cell microscopy experiments and Ofer Ovadia for assistance

REFERENCES

1. Spellman,P.T., Sherlock,G., Zhang,M.Q., Iyer,V.R., Anders,K., Eisen,M.B., Brown,P.O., Botstein,D. and Futcher,B. (1998) Comprehensive identification of cell cycle-regulated genes of the yeast saccharomyces cerevisiae by microarray hybridization. *Mol. Biol. Cell*, **9**, 3273–3297.
2. Voichek,Y., Bar-Ziv,R. and Barkai,N. (2016) Expression homeostasis during DNA replication. *Science (80-.)*, **351**, 1087–1090.
3. Hamperl,S. and Cimprich,K.A. (2016) Conflict resolution in the genome: how transcription and replication make it work. *Cell*, **167**, 1455–1467.
4. Gómez-González,B. and Aguilera,A. (2019) Transcription-mediated replication hindrance: a major driver of genome instability. *Genes Dev.*, **33**, 1008–1026.
5. García-Muse,T. and Aguilera,A. (2016) Transcription-replication conflicts: how they occur and how they are resolved. *Nat. Rev. Mol. Cell Biol.*, **17**, 553–563.
6. Brambati,A., Colosio,A., Zardoni,L., Galanti,L. and Liberi,G. (2015) Replication and transcription on a collision course: eukaryotic regulation mechanisms and implications for DNA stability. *Front. Genet.*, **6**, 166.
7. Mirkin,E. V. and Mirkin,S.M. (2005) Mechanisms of transcription-replication collisions in bacteria. *Mol. Cell. Biol.*, **25**, 888–895.
8. Prado,F. and Aguilera,A. (2005) Impairment of replication fork progression mediates RNA polII transcription-associated recombination. *EMBO J.*, **24**, 1267–1276.
9. Herrera-Moyano,E., Nia Mergui,X., García-Rubio,M.L., Barroso,S. and Aguilera,A.S. (2014) The yeast and human FACT chromatin-reorganizing complexes solve R-loop- mediated transcription–replication conflicts. *Genes Dev.*, **28**, 735–748.
10. Felipe-Abrio,I., Lafuente-Barquero,J., García-Rubio,M.L. and Aguilera,A. (2015) RNA polymerase II contributes to preventing transcription-mediated replication fork stalls. *EMBO J.*, **34**, 236–250.
11. Tuduri,S., Crabbé,L., Conti,C., Tourrière,H., Holtgreve-Grez,H., Jauch,A., Pantesco,V., De Vos,J., Thomas,A., Theillet,C. *et al.* (2009) Topoisomerase i suppresses genomic instability by preventing interference between replication and transcription. *Nat. Cell Biol.*, **11**, 1315–1324.
12. Bermejo,R., Doksani,Y., Capra,T., Katou,Y.M., Tanaka,H., Shirahige,K. and Foiani,M. (2007) Top1- and Top2-mediated topological transitions at replication forks ensure fork progression and stability and prevent DNA damage checkpoint activation. *Genes Dev.*, **21**, 1921–1936.
13. Alzu,A., Bermejo,R., Begnis,M., Lucca,C., Piccini,D., Carotenuto,W., Saponaro,M., Brambati,A., Cocito,A., Foiani,M. *et al.* (2012) Senataxin associates with replication forks to protect fork integrity across RNA-polymerase-II-transcribed genes. *Cell*, **151**, 835–846.

14. Mischo,H.E., Gómez-González,B., Grzechnik,P., Rondón,A.G., Wei,W., Steinmetz,L., Aguilera,A. and Proudfoot,N.J. (2011) Yeast sen1 helicase protects the genome from transcription-associated instability. *Mol. Cell*, **41**, 21–32.

15. Appanah,R., Lones,E.C., Aiello,U., Libri,D. and De Piccoli,G. (2020) Sen1 is recruited to replication forks via ctf4 and mrc1 and promotes genome stability. *Cell Rep.*, **30**, 2094–2105.

16. Amon,J.D. and Koshland,D. (2016) RNase h enables efficient repair of R-loop induced DNA damage. *Elife*, **5**, e20533.

17. Santos-Pereira,J.M. and Aguilera,A. (2015) R loops: new modulators of genome dynamics and function. *Nat. Rev. Genet.*, **16**, 583–597.

18. Stirling,P.C., Chan,Y.A., Minaker,S.W., Aristizabal,M.J., Barrett,I., Sipahimalani,P., Kobor,M.S. and Hieter,P. (2012) R-loop-mediated genome instability in mRNA cleavage and polyadenylation mutants. *Genes Dev.*, **26**, 163–175.

19. Soreanu,I., Hendler,A., Dahan,D., Dovrat,D. and Aharoni,A. (2018) Marker-free genetic manipulations in yeast using CRISPR/CAS9 system. *Curr. Genet.*, **64**, 1129–1139.

20. Morawska,M. and Ulrich,H.D. (2013) An expanded tool kit for the auxin-inducible degron system in budding yeast. *Yeast*, **30**, 341–351.

21. Rubner,S., Scharow,A., Schubert,S. and Berg,T. (2018) Selective degradation of Polo-like kinase 1 by a hydrophobically tagged inhibitor of the polo-box domain. *Angew. Chem. Int. Ed.*, **57**, 17043–17047.

22. Lukinavičius,G., Umezawa,K., Olivier,N., Honigmann,A., Yang,G., Plass,T., Mueller,V., Reymond,L., Corrêa,I.R., Luo,Z.G. *et al.* (2013) A near-infrared fluorophore for live-cell super-resolution microscopy of cellular proteins. *Nat. Chem.*, **5**, 132–139.

23. Donovan,B.T., Huynh,A., Ball,D.A., Patel,H.P., Poirier,M.G., Larson,D.R., Ferguson,M.L. and Lenstra,T.L. (2019) Live-cell imaging reveals the interplay between transcription factors, nucleosomes, and bursting. *EMBO J.*, **38**, e100809.

24. Brouwer,I., Patel,H.P., Meeussen,J.V.W., Pomp,W. and Lenstra,T.L. (2020) Single-Molecule fluorescence imaging in living saccharomyces cerevisiae cells. *STAR Protoc.*, **1**, 100142.

25. Carpenter,A.E., Jones,T.R., Lamprecht,M.R., Clarke,C., Kang,I.H., Friman,O., Guertin,D.A., Chang,J.H., Lindquist,R.A., Moffat,J. *et al.* (2006) CellProfiler: image analysis software for identifying and quantifying cell phenotypes. *Genome Biol.*, **7**, R100.

26. Cankorur-Cetinkaya,A., Dereli,E., Eraslan,S., Karabekmez,E., Dikicioglu,D. and Kirdar,B. (2012) A novel strategy for selection and validation of reference genes in dynamic multidimensional experimental design in yeast. *PLoS One*, **7**, e38351.

27. Dovrat,D., Dahan,D., Sherman,S., Tsirkas,I., Elia,N. and Aharoni,A. (2018) A live-cell imaging approach for measuring DNA replication rates. *Cell Rep.*, **24**, 252–258.

28. Dahan,D., Tsirkas,I., Dovrat,D., Sparks,M.A., Singh,S.P., Galletto,R. and Aharoni,A. (2018) Pif1 is essential for efficient replisome progression through lagging strand G-quadruplex DNA secondary structures. *Nucleic Acids Res.*, **46**, 11847–11857.

29. Tsirkas,I., Dovrat,D., Lei,Y., Kalyva,A., Lotysh,D., Li,Q. and Aharoni,A. (2020) Cac1 WHD and PIP domains have distinct roles in replisome progression and genomic stability. *Curr. Genet.*, **67**, 129–139.

30. Lenstra,T.L., Coulon,A., Chow,C.C. and Larson,D.R. (2015) Single-Molecule imaging reveals a switch between spurious and functional ncRNA transcription. *Mol. Cell*, **60**, 597–610.

31. Elison,G.L., Xue,Y., Song,R. and Acar,M. (2018) Insights into bidirectional gene expression control using the canonical GAL1/GAL10 promoter. *Cell Rep.*, **25**, 737–748.

32. Slubowski,C.J., Funk,A.D., Roesner,J.M., Paulissen,S.M. and Huang,L.S. (2015) Plasmids for C-terminal tagging in saccharomyces cerevisiae that contain improved GFP proteins, envy and ivy. *Yeast*, **32**, 379–387.

33. Lisby,M., Rothstein,R. and Mortensen,U.H. (2001) Rad52 forms DNA repair and recombination centers during S phase. *Proc. Natl. Acad. Sci. U.S.A*, **98**, 8276–8282.

34. Fennessy,R.T. and Owen-Hughes,T. (2016) Establishment of a promoter-based chromatin architecture on recently replicated DNA can accommodate variable inter-nucleosome spacing. *Nucleic Acids Res.*, **44**, 7189–7203.

35. Trceck,T., Chao,J.A., Larson,D.R., Park,H.Y., Zenklusen,D., Shenoy,S.M. and Singer,R.H. (2014) Single-mRNA couting using fluorescent in situ hybridization on budding yeast. *Nat. Protoc.*, **7**, 408–419.

36. Levsky,J.M. and Singer,R.H. (2003) Fluorescence in situ hybridization: past, present and future. *J. Cell Sci.*, **116**, 2833–2838.

37. Çamdere,G., Guacci,V., Stricklin,J. and Koshland,D. (2015) The ATPases of cohesin interface with regulators to modulate cohesin-mediated DNA tethering. *Elife*, **4**, e11315.

38. Bermejo,R., Lai,M.S. and Foiani,M. (2012) Preventing replication stress to maintain genome stability: resolving conflicts between replication and transcription. *Mol. Cell*, **45**, 710–718.

39. Bermejo,R., Capra,T., Gonzalez-Huici,V., Fachinetti,D., Cocito,A., Natoli,G., Katou,Y., Mori,H., Kurokawa,K., Shirahige,K. *et al.* (2009) Genome-Organizing factors top2 and hmo1 prevent chromosome fragility at sites of s phase transcription. *Cell*, **138**, 870–884.

40. Roedgaard,M., Fredsoe,J., Pedersen,J.M., Bjergbaek,L. and Andersen,A.H. (2015) DNA topoisomerases are required for preinitiation complex assembly during GAL gene activation. *PLoS One*, **10**, e0132739.

41. Azvolinsky,A., Giresi,P.G., Lieb,J.D. and Zakian,V.A. (2009) Highly transcribed RNA polymerase II genes are impediments to replication fork progression in saccharomyces cerevisiae. *Mol. Cell*, **34**, 722–734.

42. Sekedat,M.D., Fenyö,D., Rogers,R.S., Tackett,A.J., Aitchison,J.D. and Chait,B.T. (2010) GINS motion reveals replication fork progression is remarkably uniform throughout the yeast genome. *Mol. Syst. Biol.*, **6**, 353.

43. Bar-Ziv,R., Voichek,Y. and Barkai,N. (2016) Chromatin dynamics during DNA replication. *Genome Res.*, **26**, 1245–1256.

44. Bar-Ziv,R., Brodsky,S., Chapal,M. and Barkai,N. (2020) Transcription factor binding to replicated DNA. *Cell Rep.*, **30**, 3989–3995.

45. Wang,J., Rojas,P., Mao,J., Higgs,M.R., Garcia,P. and Saponaro,M. (2021) Persistence of RNA transcription during DNA replication delays duplication of transcription start sites until G2 /M. *Cell Rep.*, **34**, 108759.

46. Mirkin,E. V., Roa,D.C., Nudlet,E. and Mirkin,S.M. (2006) Transcription regulatory elements are punctuation marks for DNA replication. *Proc. Natl. Acad. Sci. USA*, **103**, 7276–7281.

47. Dutta,D., Shatalin,K., Epshtein,V., Gottesman,M.E. and Nudler,E. (2011) Linking RNA polymerase backtracking to genome instability in *E. coli. Cell*, **146**, 533–543.

48. Pomerantz,R.T. and O'Donnell,M. (2010) Direct restart of a replication fork stalled by a head-on RNA polymerase. *Science (80-)*, **327**, 590–592.

49. Churchman,L.S. and Weissman,J.S. (2011) Nascent transcript sequencing visualizes transcription at nucleotide resolution. *Nature*, **469**, 368–373.

50. Cheung,A.C.M. and Cramer,P. (2011) Structural basis of RNA polymerase II backtracking, arrest and reactivation. *Nature*, **471**, 249–253.

51. Nudler,E. (2012) RNA polymerase backtracking in gene regulation and genome instability. *Cell*, **149**, 1438–1445.

52. García-Rubio,M.L. and Aguilera,A. (2012) Topological constraints impair RNA polymerase II transcription and causes instability of plasmid-borne convergent genes. *Nucleic Acids Res.*, **40**, 1050–1064.

53. Achar,Y.J., Adhil,M., Choudhary,R., Gilbert,N. and Foiani,M. (2020) Negative supercoil at gene boundaries modulates gene topology. *Nature*, **577**, 701–705.

54. Pommier,Y., Sun,Y., Huang,S.Y.N. and Nitiss,J.L. (2016) Roles of eukaryotic topoisomerases in transcription, replication and genomic stability. *Nat. Rev. Mol. Cell Biol.*, **17**, 703–721.